

Quantitative comparison of hemodynamics in simulated and 3D angiography models of cerebral aneurysms by use of computational fluid dynamics

Tatsunori Saho^{1,2} · Hideo Onishi²

Received: 9 December 2014 / Revised: 12 April 2015 / Accepted: 16 April 2015 / Published online: 25 April 2015
© Japanese Society of Radiological Technology and Japan Society of Medical Physics 2015

Abstract In this study, we evaluated hemodynamics using simulated models and determined how cerebral aneurysms develop in simulated and patient-specific models based on medical images. Computational fluid dynamics (CFD) was analyzed by use of OpenFOAM software. Flow velocity, stream line, and wall shear stress (WSS) were evaluated in a simulated model aneurysm with known geometry and in a three-dimensional angiographic model. The ratio of WSS at the aneurysm compared with that at the basilar artery was 1:10 in simulated model aneurysms with a diameter of 10 mm and 1:18 in the angiographic model, indicating similar tendencies. Vortex flow occurred in both model aneurysms, and the WSS decreased in larger model aneurysms. The angiographic model provided accurate CFD information, and the tendencies of simulated and angiographic models were similar. These findings indicate that hemodynamic effects are involved in the development of aneurysms.

Keywords Navier–Stokes equation · Reynolds number · Finite volume · Wall shear stress · Basilar artery

1 Introduction

Arterial disease often accounts for much of infection rates and mortality. Arteriosclerosis is life-style related, and it can become fatal during the advanced stage. Arterial aneurysms that cause local distension in arteries of various sizes as well as stenosis are important pathologies. The cause of aneurysms has remained unclear, but atheroma, hypertension, and hypoplasia of connective tissue are involved [1]. Most cerebral aneurysms are saccular types that expand into one side of an arterial wall. Intra-cranial aneurysms <3 mm in diameter can be asymptomatic or can be accompanied by headache and neurologic symptoms. In 30 % of patients, cerebral aneurysms arise naturally [2], and the most common sites are the bifurcation of the middle and anterior cerebral arteries, the anterior communicating artery, and the tip of the basilar artery [3].

On the other hand, the initiation and development of aneurysms are related not only to medical factors, but also to physical factors such as wall shear stress (WSS) caused by flow dynamics that can be measured by use of computational fluid dynamics (CFD) [4–6]. Computational fluid dynamics has been simulated for engineering application [7]. However, recent advances in super-computers and image-processing workstations have led to the clinical applications of CFD [8] for visualizing blood flow and for new clinical devices. However, the clinical application of CFD has been associated with obstacles as physical properties (e.g., non-Newtonian fluid, rigid wall, and inlet velocity condition) [9–11].

Three-dimensional (3D) images have been reconstructed by cone-beam computed tomography (CBCT) by use of a flat-panel detector (FPD) for angiography, which is indispensable for treatment of cerebral aneurysms [12]. Reconstructed 3D images could be observed from several

✉ Tatsunori Saho
sahotatsu@gmail.com

Hideo Onishi
onisi@pu-hiroshima.ac.jp

¹ Department of Radiological Technology, Kokura Memorial Hospital, 3-2-1 Asano Kitakyusyu, Fukuoka 802-8555, Japan

² Program in Biological System Sciences, Graduate School of Comprehensive Scientific Research, Prefectural University of Hiroshima, 1-1 Gakuenmachi Mihra, Hiroshima 723-0053, Japan

directions, and they have played a role in the selection of appropriate treatment strategies [13]. Furthermore, CFD analyses by use of 3D magnetic resonance angiography (MRA) images have proved valuable [14–17]. Saho et al. [18] uncovered a relationship between carotid stenosis and hemodynamics, which indicated that the development of cerebral aneurysms was associated with hemodynamics in the same manner as carotid stenosis [19].

The CFD study was performed with MRA images in a previous study. The spatial resolution of MRA image, however, is approximately around 1 mm, which is not adequate to detect the small cerebral arterial aneurysm. Accordingly, we tried to work on the concern about in 3D-image reconstruction with FPD angiography that had about 0.3 mm spatial resolution. Angiography generally became popular as compared with MRA. To our knowledge, this is the first study which used 3D-angiography with FPD. We evaluated hemodynamics at the tip of the basilar artery using CFD simulations with known geometry and a 3D angiographic model based on patient-specific medical images to determine how cerebral aneurysms develop.

2 Materials and methods

2.1 Study design

Simulated and angiographic models were analyzed by CFD. Simulated models comprised aneurysms of various sizes located at the tip of the basilar artery, and a 3D rotational angiographic mode was based on an aneurysm in one patient that was also located at the basilar artery tip.

2.2 Analysis of computational fluid dynamics (CFD)

We built a CFD system based on a Z220 CMT workstation (Hewlett Packard, Palo, CA, USA) to improve the computing performance [18]. Medical images obtained by 3D angiography were exported as stereolithography (STL) files. Finite volume mesh generation, determination of boundary conditions, and CFD analysis proceeded by use of OpenFOAM (Open CFD Ltd., Bracknell, UK) [20], and the results were visualized by use of Paraview (Kitware, Inc., Clifton Park, NY, USA). We refer here to the CFD analysis as “pre-processing”, and visualization as “post-processing”. Figure 1 shows a flow chart of the analysis.

2.3 Simulated basilar tip aneurysm models

We constructed simulated basilar tip models of aneurysms to evaluate aneurysm formation. Simulated models (diameters of parent and branch vessels 5 and 3 mm,

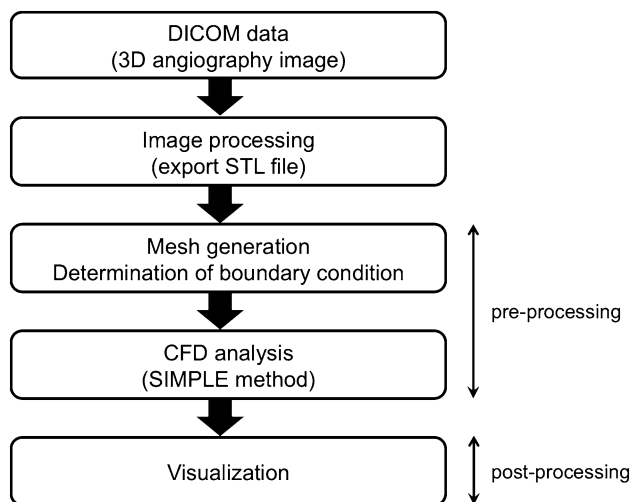


Fig. 1 Flow chart of analysis. The surface rendering image processed by Osirix, and output as stereolithography (STL) file images. Finite volume elements based on STL files were created with OpenFOAM as CFD analysis software. Boundary conditions were provided by the graphical user interface Helyx OS for OpenFOAM. Results were validated and visualized by Paraview

respectively) supposed an aneurysm of the basilar artery prepared by free computer-aided design (<http://www.freecadweb.org>), offset spheres (3 and 10 mm) on the basilar tip. Figure 2 shows simulated models.

2.4 Patient history

A patient diagnosed with an intra-cranial aneurysm was retrospectively identified and recruited with appropriate ethical approval from the Kokura Memorial Hospital clinical research review committee. Angiographic images were obtained under conventional trans-femoral catheterization of the cerebral blood vessels.

2.5 Three-dimensional rotational angiographic model

Data were acquired with an angiography system [Allura Xper FD 20/20 (Philips Healthcare, Best, The Netherlands)]. Rotational angiographic images (85 kVp, 176 mA, 7 ms, 30 frame/s) were acquired over a period of 4.1 s with C-arm rotation of 240° after 14 mL of nonionic contrast material (300 mg iodine/mL) was injected over a period of 6 s into the vertebral artery. The corresponding projection images were reconstructed into a 3D dataset of 512 × 512 × 512 isotropic voxels (0.3 mm) and a 150-mm field of view on a dedicated Philips workstation. Considering the convergence of the computing process and the cost, the distal branches were truncated by use of Osirix (Osirix Foundation, Geneva, Switzerland) [20]. Figure 3 shows the maximum intensity projection (MIP) images and

Fig. 2 Illustration of basilar artery models. Diameters of main trunk and branches are 5 and 3 mm, respectively. Normal basilar artery (a), basilar arteries with small (b) and large (c) aneurysms (3 and 10 mm, respectively) at basilar tip

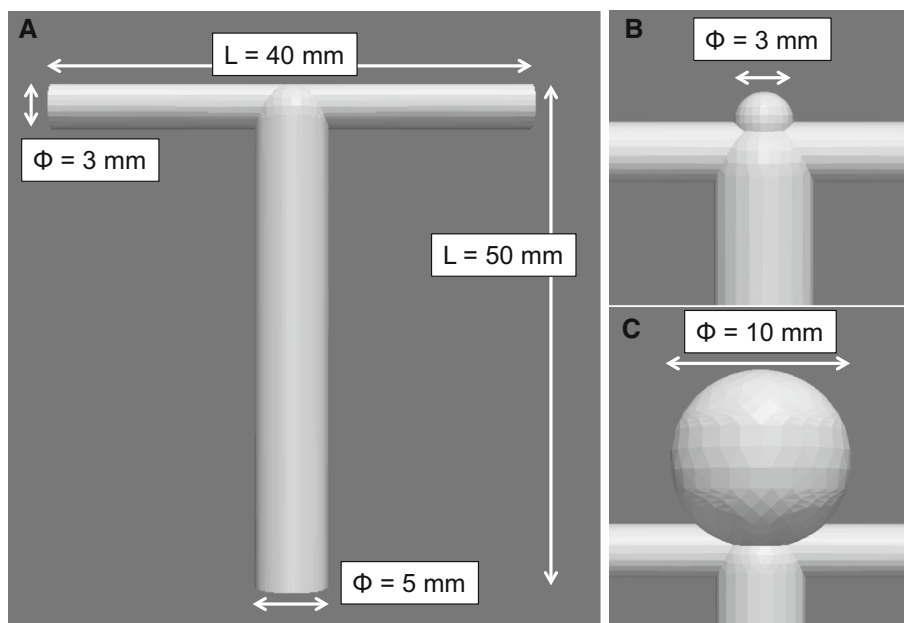
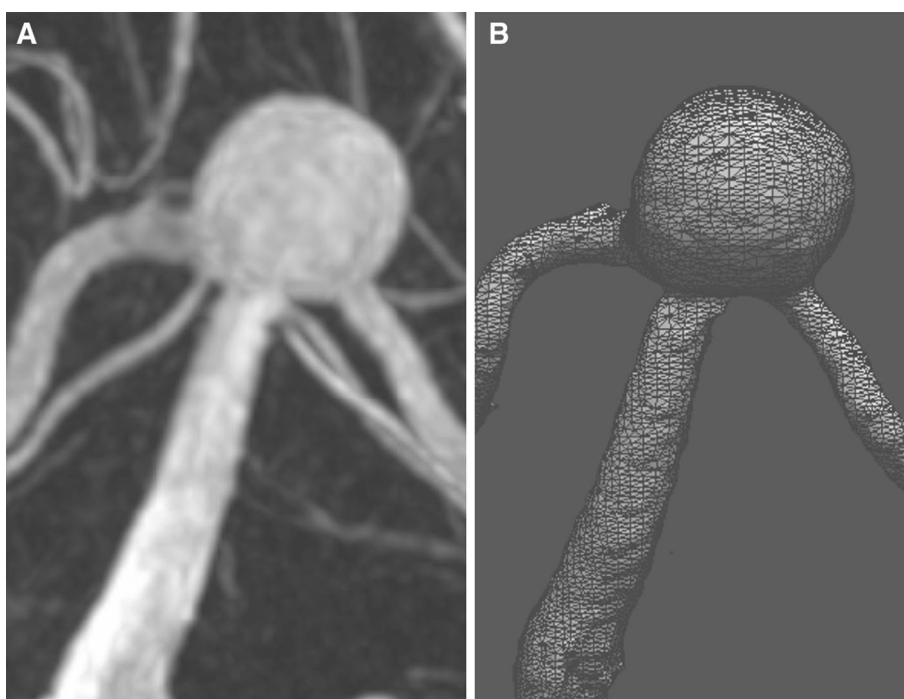


Fig. 3 Patient-specific CFD analysis models. **a** Three-dimensional angiographic image acquired with selective intra-arterial injection of contrast agent. **b** Vascular stereolithography (STL) model of cerebral aneurysm reconstructed from 3D rotational angiography image



the STL model obtained by 3D rotational angiography. The STL files are described only as geometric data that allow complete anonymity.

2.6 CFD modeling

The simulated and angiographic models were analyzed by CFD. Regions of interest were separated into hexahedral elements by use of a “blockMesh” tool in the OpenFOAM, and the surfaces of subjects were determined by use of

“snappyHexMesh” tool in the OpenFOAM. We created three layers that would improve the accuracy near the vessel wall.

After finite volume elements were created, boundary conditions (inlet plane, outlet plane, and wall) and fluid rheology were determined by use of Helyx OS (Engys Ltd., London, UK). Table 1 shows the conditions of the CFD analysis. Blood is generally considered to be a non-Newtonian fluid. We assumed that blood is an incompressible Newtonian fluid, with density and viscosity of 1050 kg/m^3

Table 1 Analytical condition

Parameters	Preset value
Fluid density (kg/m ³)	1050
Fluid viscosity (Pa s)	0.004
Flow rate (m/s)	0.8
Wall condition	Rigid and no-slip
Solving method	SIMPLE method

and 4.0×10^{-3} Pa s, respectively [21]. We also assumed that the vessel walls were rigid, and no-slip boundary conditions were applied at the walls. The input flow was steady at the inlet plane, and the flow velocity was 0.8 m/s [23].

Fluid rheology was needed distinguishing between laminar and turbulent flow in the CFD analysis. Reynolds numbers (Re) representing fluid properties were calculated as:

$$Re = \frac{\rho v L}{\mu} \quad (1)$$

where ρ represents density, v is the velocity, L is a characteristic linear dimension and μ is viscosity. The calculated Reynolds numbers of the simulated and angiographic models were 1050 and 840, respectively. Flow is generally turbulent at Reynolds numbers >2000 . However, the Reynolds numbers in both models in the present study were <2000 . Therefore, we performed a CFD analysis for laminar flow. Blood flow was modeled as an incompressible Newtonian fluid as described by Navier–Stokes equations in 3D. The semi-implicit method for pressure-linked equations (SIMPLE) method was used for the computational scheme [23, 24]. Wall shear stress acted in parallel with the vessel wall, and was calculated as:

$$\vec{\tau} = \mu \frac{\Delta \vec{u}}{\Delta z} \quad (2)$$

where $\vec{\tau}$ represents wall shear stress, μ is the viscosity, \vec{u} is the velocity (parallel to the wall), and z is distance from the wall. The analytical results were visualized by use of Paraview software, and the stream line and distribution of wall shear stress were evaluated.

3 Results

3.1 Mesh generation

Table 2 shows that the number of finite volume elements generated by the simulated and angiographic models was of the order of 10^6 and 10^5 , respectively, and processing time becomes too long and increased elements. Figure 4

Table 2 Number of elements and time required for generation of elements in both models

Model	Number of elements	Mesh generation time (s)
Healthy basilar artery	1,158,404	155.0
Aneurysm, 3 mm	1,109,183	205.6
Aneurysm, 10 mm	1,214,875	257.4
3D angiography	320,899	124.9

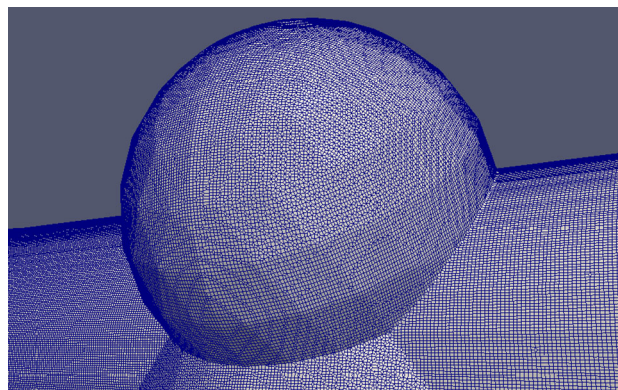


Fig. 4 Analysis model for creation of computational mesh. The volume comprised finite volume elements, and three layers were added to the vessel wall as a boundary layer

shows the results of mesh generation in the simulated model.

3.2 CFD analysis for the simulated model

Figures 5 and 6 show the results of the CFD analysis with use of the simulated model. Figure 5 also shows the stream line at aneurysms in each model. The velocity decreased at the basilar tip of the model of a normal basilar artery. The intra-aneurysmal flow velocity was decelerated, particularly in large aneurysms in which the stream line formed a complex vortex flow. Therefore, the mean WSS in each model appeared at the basilar tip and at the aneurysmal surface. In particular, the ratio of WSS in the region of large model aneurysms was 10 % of that in the basilar artery.

3.3 CFD analysis with use of angiographic model

Figures 7 and 8 show the results of CFD analysis by use of the angiographic model. Figure 7 shows the stream line for this model, in which vortex flow was found in the same aneurysmal region as that in the simulated model aneurysm. Blood flowed from the parent vessel along the posterior wall into the tip and anterior side of the aneurysm,

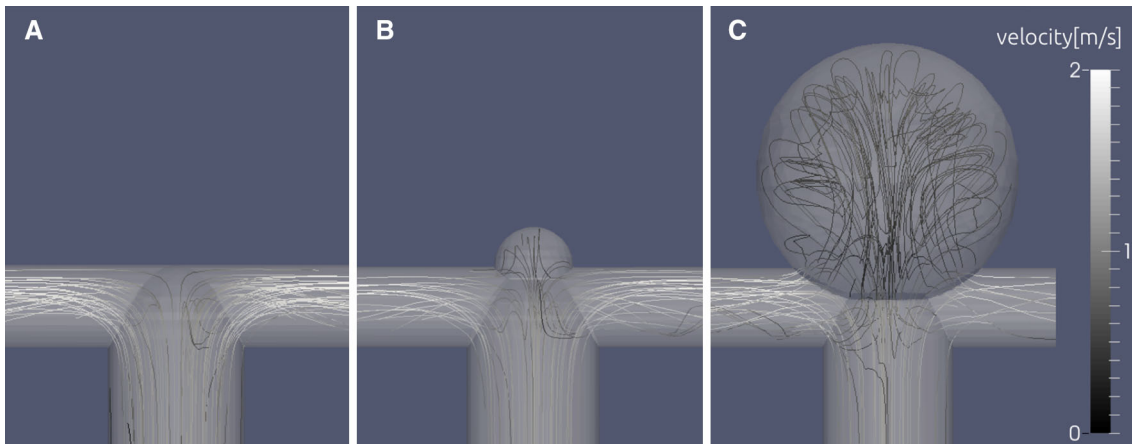


Fig. 5 Visualization of stream lines for simulated basilar artery models. **a** Normal basilar artery model. Basilar arteries with small (3 mm, **b**) and large (10 mm, **c**) at tip. Stream lines are *gray-scaled*

according to velocity magnitude. Decelerated flow velocity at basilar tip and intra-aneurysmal vortex

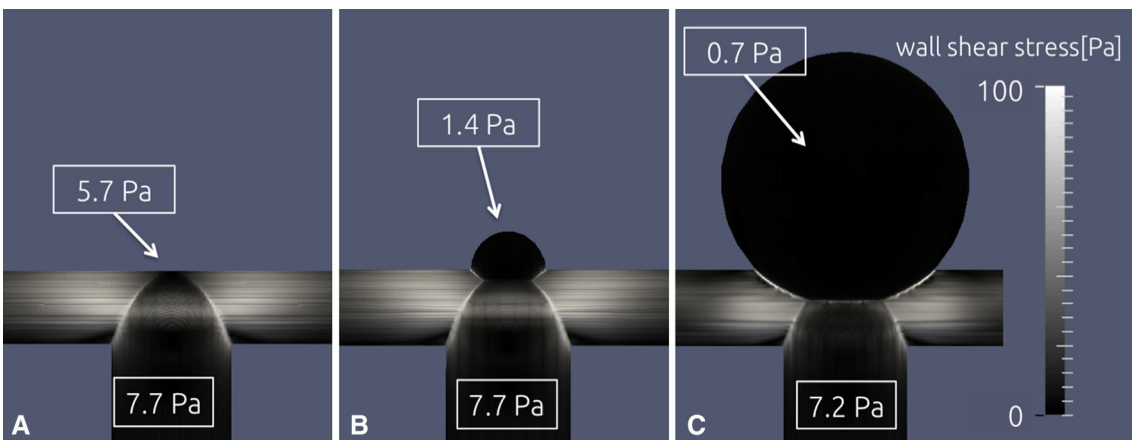
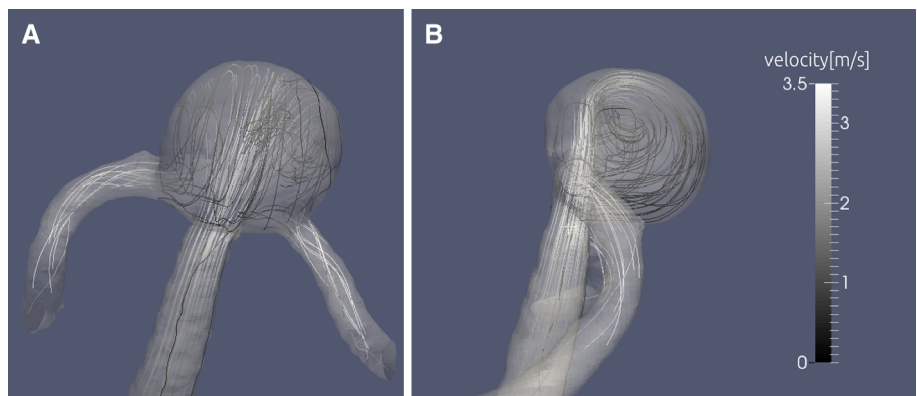


Fig. 6 Visualization of wall shear stress (WSS) in basilar artery models. Model of normal basilar artery (**a**). Basilar artery with small (3 mm, **b**) and large (10 mm, **c**) aneurysms at basilar tip. Wall shear

stress is *gray-scaled* according to magnitude. That at basilar tip is decreased slightly compared with the parent vessel, and the aneurysmal WSS is significantly decreased

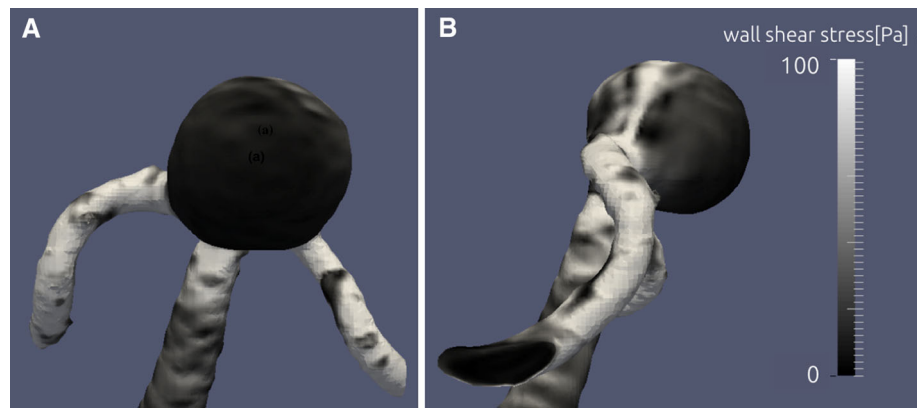
Fig. 7 Visualization of stream lines for angiography models. Anterior (**a**) and lateral (*right side* **b**) views. Stream line is *gray-scaled* according to magnitude of velocity. Flow velocity is decelerated at anterior and center regions of aneurysm, and intra-aneurysmal flow is vortex



resulting in vortex flow. The blood then flowed out of the aneurysm, became distributed between two branch vessels, and did not flow against the stream line toward the parent

vessel. The blood flow velocity of 3 m/s into the tip of the aneurysm decelerated to 1 m/s at the anterior side and center of the aneurysm. Figure 8 shows that the WSS at the

Fig. 8 Anterior (a) and lateral (right side b) views. Stream line and WSS are gray-scaled according to magnitude of velocity. Wall shear stress is remarkably decreased at the anterior region of the aneurysm



anterior side of the angiographic model aneurysm was about 5 % of that of the mean WSS in the basilar artery (8.2 vs 150 Pa).

4 Discussion

Commercial software has generally been used for CFD analysis. Constructing a system with use of the open source software, we spent more cost on hardware to improve analytical precision.

A finite volume mesh was generated within 250 s in the model with over 10^6 elements. Previously, >1000 s were required to generate a finite volume mesh in a simplified cylinder model [18]. Thus, the amount of time required to generate a mesh was efficiently reduced by 25 % by the high-performance system.

The CFD analysis proceeded with many approximations. The original geometry was continued in the reconstructed model analysis. However, a truncation error arose when discretization resulted in a finite volume, which was one of the approximations. A large truncation error that could not be ignored would result in critical computing errors in the results for regions of interest. A previous study has shown that the spatial resolution of MR angiography is about 1 mm [18]. In contrast, that of 3D angiography was 0.3 mm in this study, which represented an approximately threefold improvement. The reproducibility of the carotid bifurcation, even on MRA images, was reasonable, but insufficient for reconstruction of a 2–3 mm intra-cranial aneurysm. The region of interest was very small in this study; 3D angiography with FPD could clearly visualize small aneurysmal blebs [20]. Therefore, computational models based on 3D angiography are useful for accurate CFD analysis.

We evaluated the process of aneurysm formation and development using CFD analyses of simulated models (normal artery, 3 and 10 mm aneurysms). The basilar

artery tip was the preferred site of aneurysm formation. Blood flowing from the basilar artery collided with the rectangular basilar tip and then became distributed to the left and right posterior cerebral artery, resulting in complex vortex flow at the basilar tip. Complex vortex and decreased flow in the same area of the stream line were caused by the extent of the hydraulic diameter with branches and the aneurysm. Therefore, the Reynolds number increased and the flow features started to destabilize and resemble those of turbulent flow, thus increasing the aneurysm formation.

Evaluation of the flow dynamics in the basilar artery was important for deriving information as to how aneurysms are formed. A previous study showed that the decreasing WSS affects atherosclerosis. The present study showed that WSS in a 10 mm aneurysm was about one tenth of that of the basilar artery, and that the WSS decreased as the aneurysm became larger. Here, we evaluated an aneurysm that developed in a patient who had atherosclerosis. We considered that this aneurysm was associated with the atherosclerosis, because the low WSS in the specific region caused the appropriate conditions for an intra-cranial aneurysm to develop.

The WSS was low at the aneurysmal region in the 3D angiographic and simulated models, and intra-aneurysmal blood flowed as a vortex in the posterior to anterior direction. Most previous studies have analyzed CFD after aneurysms had formed, whereas we reconstructed simulation models before they formed and found a low WSS at the basilar tip. Our results indicated that aneurysms form at regions of low WSS, and that such formation further decreases the WSS.

The aneurysm expanded into the region of low WSS in the angiographic model, which showed an association of hemodynamics with aneurysm development. However, we analyzed only one patient in this study, and future studies should use CFD to determine the risk of aneurysmal rupture.

5 Limitations

The fact that hemodynamics obtained by use of CFD is consistent with in vivo images obtained by MRA is widely accepted. Moreover, progress in hardware and calculation algorithms allowed in to make the simulation precise. However, this fine analysis has a high computational cost. Hence, previous computations have been based on many assumptions that were also included herein for simplification. This led to errors based on the following approximations: Newtonian dynamics, steady flow, and discretization of the analysis domain. The flow dynamics rendered herein represent only a snapshot of the hemodynamic stresses imposed on a specific aneurysm. Transposing a continuous phenomenon to a discrete field introduces many approximations and errors, as described. However, the advantage of CFD modeling is the ease of changing boundary conditions and the ability to reproduce the phenomena in vivo. The significant practical limitations of the modeling described here should be resolved before hemodynamics can be derived.

6 Conclusions

We used CFD to analyze a simulated model of basilar tip aneurysms with fundamental geometry. Low WSS and decreased velocity were evident at the bifurcation of the basilar artery in the normal model, at the preferred site for aneurysm formation. Vortex flow was identified in aneurysms, and the WSS was low in larger model aneurysms.

Patient-specific CFD analysis based on 3D angiography allowed accurate reconstruction of the original geometry of a patient. The direction of aneurysmal expansion and the low WSS in the same regions in the angiographic and the simulated model suggested that hemodynamics affects the development of cerebral aneurysms.

Conflict of interest The authors declare that they have no conflict of interest.

References

1. Kumar V, Cotran SR, Robbins LS. Robbins basic pathology. 7th ed. Philadelphia: Elsevier Saunders; 2003. p. 409–54.
2. Nagahiro S, Satoh K, Nakajima N, Hamada J, Ushio Y. Growth mechanism and treatment of partially thrombosed giant aneurysm. *Jpn J Neurosurg.* 2001;10:10–7.
3. Yasukawa K, Kamijo Y, Momose G, Kobayashi S, Ikeda A. A case of anterior cerebral artery dissecting aneurysm presenting subarachnoid hemorrhage and cerebral infarction at the same time. *Surg Cereb Stroke.* 1993;21:461–6.
4. Hoi Y, Meng H, Woodward SH, Bendok BR, Hanel RA, Guterman LR, Hopkins LN. Effects of arterial geometry on aneurysm growth: three-dimensional computational fluid dynamics study. *J Neurosurg.* 2004;101:676–81.
5. Nakatani H, Hashimoto N, Kang Y. Cerebral blood flow patterns at major vessel bifurcations and aneurysms in rats. *J Neurosurg.* 1991;74:258–62.
6. Gonzalez CF, Choi YI, Ortega V. Intracranial aneurysms: flow analysis of their origin and progression. *Am J Neuroradiol.* 1992;13:181–8.
7. Jameson A, Martinelli L, Pierce NA. Optimum aerodynamic design using the Navier-Stokes equations. *Theoret Comput Fluid Dyn.* 1998;10:213–37.
8. Endo T, Matsuoka S, Hashizume N, Nagasaka M. Performance evaluation of TSUBAME heterogeneous supercomputer with linpack. *Inf Process Soc Jpn.* 2007;48:62–70.
9. Zhang Y, Furusawa T, Sia SF, Umezu M, Qian Y. Proposition of an outflow boundary approach for carotid artery stenosis CFD simulation. *Comput Methods Biomech Biomed Eng.* 2013;16:488–94.
10. Steinman D, Milner J, Norley JC, Lownie S, Holdsworth WD. Image-based computational simulation of flow dynamics in a giant intracranial aneurysm. *Am J Neuroradiol.* 2003;24:559–66.
11. Papanthanasopoulou P, Zhao S, Köhler U, Robertson MB, Long Q, Hoskins P, Xu XY, Marshall I. MRI measurement of time-resolved wall shear stress vectors in a carotid bifurcation model, and comparison with CFD predictions. *J Magn Reson Imag.* 2003;17:153–62.
12. Raj S, Irani FG, Tay KH, Tan BS. C-arm cone beam computed tomography: a new tool in the interventional suite. *Ann Acad Med.* 2013;42:585–92.
13. Fiorella D, Arthur A, Schafer S. Minimally invasive cone beam CT-guided evacuation of parenchymal and ventricular hemorrhage using the Apollo system: proof of concept in a cadaver model. *J NeuroIntervent Surg.* 2014;0:1–5. doi:10.1136/neurintsurg-2014-011293.
14. White PM, Wardlaw JM. Unruptured intracranial aneurysms. *J Neuroradiol.* 2003;30:336–50.
15. Ujiie H, Tamano Y, Sasaki K, Hori T. Is the aspect ratio a reliable index for predicting the rupture of a saccular aneurysm? *Neurosurgery.* 2001;48:495–503.
16. Ma B, Harbaugh RE, Raghavan ML. Three-dimensional geometrical characterization of cerebral aneurysms. *Ann Biomed Eng.* 2004;32:264–73.
17. Millan D, Dempere ML, Pozo JM, Cebral JR, Frangi AF. Morphological characterization of intracranial aneurysms using 3-D moment invariants. *IEEE Trans Med Imag.* 2007;26:1270–82.
18. Saho T, Onishi H, Sugihara T, Nakamura Y, Yuda I. Tackling hemodynamic analysis of the carotid artery using open-source software and computational fluid dynamics. *Jpn J Radiol Technol.* 2012;69:1241–9.
19. Nixon AM, Gunel M, Sumpio BE. The critical role of hemodynamics in the development of cerebral vascular disease. *J Neurosurg.* 2010;112:1240–53.
20. The OpenCFD Foundation. OpenFOAM Users Guide Ver 2.3.1 3rd December 2014. Paris: OpenCFD Foundation; 2014.
21. Castro MA, Putman CM, Cebral JR. Computational fluid dynamics modeling of intracranial aneurysms: effects of parent artery segmentation on intra-aneurysmal hemodynamics. *Am J Neuroradiol.* 2006;27:1703–9.
22. Yamamoto S, Maruyama S, Nakahara Y, Yoneyama S, Tanifuji S, Wada S, Hamada S, Komizu M, Johkoh T, Yamaguchi M, Doi M, Yamaguchi T. Abdominal aortic aneurysm using multislice computed tomography. Computed flow dynamics in abdominal aortic aneurysm using multislice computed tomography. *Jpn J Radiol Technol.* 2006;62:115–21.

23. Soustiel FJ, Shik V, Shreiber R, Tavor Y, Goldsher D. Basilar vasospasm diagnosis investigation of a modified "Lindegaard Index" based on imaging studies and blood velocity measurements of the basilar artery. *Stroke*. 2002;33:72–8.
24. Caretto LS, Gosman AD, Patankar SV, Spalding DB. Two calculation procedures for steady, three-dimensional flows with recirculation. *Third Int Conf Numer Methods Fluid Mech*. 1973;19:60–8.
25. Yin R, Chow KW. Comparison of four algorithms for solving pressure-velocity linked equations in simulating atrium fire. *Int J Archit Sci*. 2003;4:24–35.